

Atomic and magnetic structures of $(\text{CuCl})\text{LaNb}_2\text{O}_7$ and $(\text{CuBr})\text{LaNb}_2\text{O}_7$: Density functional calculations

Chung-Yuan Ren^{a,†} and Ching Cheng^b

^a *Department of Physics, National Kaohsiung Normal University, Kaohsiung 824, Taiwan*

^b *Department of Physics, National Cheng Kung University, Tainan 701, Taiwan*

† *E-mail address: cyren@ncku.edu.tw*

Abstract

The atomic and magnetic structures of $(\text{Cu}X)\text{LaNb}_2\text{O}_7$ ($X=\text{Cl}$ and Br) are investigated using the density-functional calculations. Among several dozens of examined structures, an orthorhombic distorted 2×2 structure, in which the displacement pattern of X halogens resembles the model conjectured previously based on the empirical information is identified as the most stable one. The displacements of X halogens, together with those of Cu ions, result in the formation of $X\text{-Cu-X-Cu-X}$ zigzag chains in the two materials. Detailed analyses of the atomic structures predict that $(\text{Cu}X)\text{LaNb}_2\text{O}_7$ crystallizes in the space group $Pbam$. The nearest-neighbor interactions within the zigzag chains are determined to be antiferromagnetic (AFM) for $(\text{CuCl})\text{LaNb}_2\text{O}_7$ but ferromagnetic (FM) for $(\text{CuBr})\text{LaNb}_2\text{O}_7$. On the other hand, the first two neighboring interactions between the Cu cations from adjacent chains are found to be AFM and FM respectively for both compounds. The magnitudes of all these in-plane exchange couplings in $(\text{CuBr})\text{LaNb}_2\text{O}_7$ are evaluated to be about three times those in $(\text{CuCl})\text{LaNb}_2\text{O}_7$. In addition, a sizable AFM inter-plane interaction is found between the Cu ions separated by two NbO_6 octahedra. The fourth-neighbor interactions are also discussed. The present study strongly suggests the necessity to go beyond the square $J_1 - J_2$ model in order to correctly account for the magnetic property of $(\text{Cu}X)\text{LaNb}_2\text{O}_7$.

PACS: 71.15.Mb, 75.45.+j

I. INTRODUCTION

Low-dimensional quantum spin systems with frustrated interactions have drawn considerable attention for several decades [1]. In particular, the square-lattice $S = 1/2$ frustrated Heisenberg magnets with first-neighbor exchange constant J_1 and second-neighbor constant J_2 are increasingly interesting due to their unusual ground states and quantum phenomena [2]-[13]. Based on the $J_1 - J_2$ model studies, there exist several phases as a function of J_2/J_1 . When J_1 dominates or J_2 is ferromagnetic (FM), the system is either Néel antiferromagnetic (NAFM) or FM depending on the sign of J_1 (Refs. [3, 7, 12, 13]). When J_2 is antiferromagnetic (AFM) and dominates, there appears the so-called columnar AFM (CAFM) order [3, 7] with antiferromagnetically coupled FM chains. The CAFM and FM, or CAFM and NAFM ordered phases are separated by the intermediate quantum-disordered phases, the nature of which is not yet fully resolved [2, 4-7, 12, 13]. The recent discoveries of quasi-two-dimensional materials are realizations to test the validity of the $J_1 - J_2$ model. Prominent among them are $\text{Li}_2\text{VO}(\text{Si,Ge})\text{O}_4$ (Refs. [14, 15]), $AB(\text{VO})(\text{PO}_4)_2$ ($A, B = \text{Pb, Zr, Sr, Ba}$) (Refs. [16-18]), $(\text{CuBr})A'_2B'_3\text{O}_{10}$ ($A' = \text{Ca, Sr, Ba, Pb; } B' = \text{Nb, Ta}$) (Ref. [19]), and $(\text{Cu}X)\text{LaNb}_2\text{O}_7$ ($X = \text{Cl, Br}$) (Refs. [20, 21]). $(\text{Cu}X)\text{LaNb}_2\text{O}_7$ compounds are of particular interest because they allow systematic tuning and understanding of the structural and magnetic properties, which are plausibly connected with the phenomenon of high- T_c superconducting cuprates.

Although divalent copper with the electronic configuration d^9 should be Jahn-Teller active and lead to the cooperative lattice distortion (e.g., perovskite KCuF_3 (Ref. [22])), the precise crystal structure of the layered copper oxyhalides $(\text{Cu}X)\text{LaNb}_2\text{O}_7$ is still under debate. Earlier structural studies on $(\text{Cu}X)\text{LaNb}_2\text{O}_7$ were carried out with the tetragonal space group P_4/mmm , where the Cu and X sites possess the C_4 symmetry [23, 24]. While the Rietveld refinement gave satisfactory results, the thermal parameter for halogens remained large. Besides, in this structure copper is in a significantly squeezed octahedral coordination with two short Cu-O bonds (about 1.9 Å) and four rather long Cu-X bonds (2.7 Å), which are also quite unusual. Subsequently, the neutron diffraction experiment [25] proposed that the Cl ions in $(\text{CuCl})\text{LaNb}_2\text{O}_7$ ($(\text{CuCl})\text{LNO}$) shifted away from the ideal Wyckoff $1b$ position [23]. The transmission electron microscopy measurement on $(\text{CuCl})\text{LNO}$ (Ref. [20]) revealed superlattice reflections corresponding to an enlarged 2×2 unit cell. The nuclear

magnetic resonance and the nuclear quadrupole resonance experiments for (CuCl)LNO and (CuBr)LaNb₂O₇ ((CuBr)LNO) further demonstrated the lack of the tetragonal symmetry at both Cu and Cl/Br sites [20, 21].

The magnetic properties of (CuCl)LNO and (CuBr)LNO are also unusual and lack a clear microscopic interpretation. The former exhibits a spin liquid phase with a spin gap [20, 26, 27] that are incompatible [28] with the square $J_1 - J_2$ model. On the other hand, it has been reported [29] that the replacement of Cl by Br leads to a CAFM order in (CuBr)LNO at low temperatures. However, it is unclear whether the Cu ions connected with the dominant exchange interaction couple ferromagnetically or antiferromagnetically [21]. Moreover, both (CuCl)LNO and (CuBr)LNO are claimed to be FM J_1 compounds [27, 29] whose justifications largely rely on the $J_1 - J_2$ model. Yet, the structural study [21] raised doubts over the validity of the model. Therefore, unambiguous determination of the crystal structure is crucial for understanding these complex systems.

At present, there are several structural models proposed for the CuX plane. Whangbo and Dai [28] suggested a model that consists of different ring clusters to explore the exchange couplings. However, the existence of inequivalent Cu and Cl sites in such a model is in contradiction to the experimental results that both Cu and X occupy a unique crystallographic site with no substantial disorder [20, 21]. Yoshida *et al.* [20], based on the empirical evidence, proposed an orthorhombic distorted 2×2 structure (hereafter referred to as the YY model). In this model, the displacement of Cl ions generates different exchange couplings among the nearest neighboring Cu pairs. A Cu dimer formed by the dominant exchange interaction was considered [20] to study the spin-gap behavior. The same structural model was shown [21] to consistently account for (CuBr)LNO. The third model, suggested by Tsirlin and Rosner (TR) [30] is also characterized by an ordering pattern but with a 2×1 periodicity, where the local environment of copper is distorted to form the CuO₂Cl₂ plaquette.

First-principles calculations have proven to be an appealing method to deal with complex systems [31–33]. Such a method can efficiently and reliably calculate the total energy, which is crucial in determining the most stable structure in order to study all relevant physical properties. In this work, we will investigate the atomic structure and resultant magnetic property of (CuCl)LNO and (CuBr)LNO based on the density functional theory. Our results show that, among several dozens of examined structures, the distortion pattern of the most

stable one is similar to that of the YY model. The displacement of the X ions changes the environment of copper to form the CuO_2X_2 plaquette. In addition, these two materials crystallize in the space group $Pbam$. The FM chains in CAFM (CuBr)LNO are found to be along the direction which is contrary to the previous conjecture [21]. It will be shown that (CuCl)LNO still belongs to the AFM J_1 compound. The first- and second-neighbor exchange couplings of (CuCl)LNO and (CuBr)LNO are also discussed in detail.

II. CRYSTAL STRUCTURE AND COMPUTATIONAL DETAILS

Figure 1 illustrates the basic crystal structure of the copper oxyhalides $(\text{CuX})\text{LaNb}_2\text{O}_7$. It is made up of copper-halogen planes and nonmagnetic double-perovskite LaNb_2O_7 slabs. The La ions are located at the 12-coordinate sites of the double-perovskite slabs. The CuX planes and the LaNb_2O_7 slabs alternate along the c direction such that the copper is six-fold coordinated, bridging between the apical O ions of NbO_6 octahedra and surrounded by four X halogens. Because of the short Cu-O bond length (~ 1.9 Å), the CuX plane is more appropriately considered as a CuXO_2 layer. The initial structural study on $(\text{CuX})\text{LaNb}_2\text{O}_7$ was carried out with the space group P_4/mmm , where both Cu and X have the C_4 symmetry [23, 24]. In this model (hereafter referred to as C4), the Cu and X ions are located at the Wyckoff $1d$ and $1b$ positions, respectively (Fig. 2(a)). Later studies [20, 25] proposed that Cl ions are displaced from the C_4 -symmetry positions. The YY 2×2 model is represented in Fig. 2(b). The displacement of X ions on the CuX plane leads to the formation of the $X\text{-Cu-X-Cu-X}$ zigzag chains, as indicated in Fig. 2(b). The original equivalent and perpendicular Cu chains are now distinguishable. Here, the direction extending along the zigzag chains is defined as the b axis.

The present calculations were based on the generalized gradient approximation (GGA) [34] to the exchange-correlation energy functional of the density functional theory. It is known [35–37] that Cu-derived oxide compounds are usually strongly correlated systems. The correlation effect is important for the present systems to understand their ground state. Therefore, the on-site Coulomb interaction U for Cu $3d$ electrons was also included [22] (GGA+ U) in this work. Since the on-site exchange interaction J is expected to be less influenced by the solid state effects [30], the relation $J = 0.1U$ was used [38] for different choices of U . The projector-augmented-wave potentials, as implemented in VASP [39, 40],

were employed for the interactions between the ions and valence electrons. The plane-wave basis set with an energy cut-off of 500 eV was used. To minimize numerical uncertainties, structural optimizations were performed using a 2×2 supercell for all the test structures unless specified otherwise. The $6 \times 6 \times 4$ Monkhorst-Pack grids were taken to sample the corresponding Brillouin zone. The lattice parameters and atomic positions were relaxed until the total energy changed by less than 10^{-6} eV per conventional cell and the residual force was smaller than 0.01 eV/Å.

III. RESULTS AND DISCUSSION

A. Energetics

We first calculated the total energies of the C4 structure and several 2×1 and 2×2 distorted structures with different displacement patterns of the X halogens. The YY 2×2 model is found to be the most stable one. As compared to the C4 structure, the YY model has a significant 0.3 and 0.2 eV/fu lowering in the energy of (CuCl)LNO and (CuBr)LNO, respectively. This directly rules out the possibility that the two compounds crystallize in the C_4 symmetry. Particularly, over the full U range from 0 eV to 8 eV, the YY model is 0.1 eV/fu lower than the TR 2×1 model (see Fig. 4 in Ref. [30]) for both materials. The nonmagnetic calculations with and without U lead to the same conclusion. Therefore, *the structural distortion outweighs the magnetism and on-site correlation effects* in determining the atomic structure. Note that, besides Refs. [20] and [21], very recent experimental evidences [41] also confirm that the original unit cell should be double along both the a and b axes for the family of these compounds. Our study therefore provided theoretical support for the stabilization of the YY 2×2 model.

To examine whether there exists other more stable structure with the X ions restricted to the Cu plane, we perform the calculations for (CuCl)LNO with twenty sets of random displacements of all four Cl ions from the positions in the YY model. However, no such structure was found. The resultant configurations of the trial structures are either relaxed back to the YY model or trapped into a nearby higher energy minimum.

Next, we allow the halogens in the YY model to move off the plane. It is found that the X ions in the relaxed structures are $0.02 - 0.04$ Å away from the Cu plane. However, the

change in the total energy is rather small. At $U=0$ and 8 eV, the results of both materials show that the energy differences are only within 2 meV per 2×2 supercell while the energies for the structures with the X ions fixed in the plane remain lower. We also examine the two structures in Figs. 16(e) and 16(f) of Ref. [20], which are based on another 2×2 configuration with the Cl ions displaced away from the Cu plane in a different way. The calculations indicate that, after relaxation, both are energetically about 0.2 eV/fu higher than the YY model. The increase in the total energy mostly comes from the different in-plane structural distortions. Again, the contribution from the z -component shift of Cl ions is rather minor. Hence, the distortion on the CuX plane is predominantly crucial to stabilize the atomic structure. In the following discussion, we shall focus on the YY model with X ions kept in the Cu plane [42].

Now, we analyze the total energies influenced by the on-site Coulomb interaction and the different magnetic configurations shown in Fig. 3. Here, SC1 and SC3 are FM and NAFM. SC2 and SC4 are both CAFM, with the FM chain along the b and a directions, respectively. The results are displayed in Fig. 4, where the energy of SC2 was chosen as a reference. For (CuCl)LNO, the energies of SC1, SC2, and SC4 are very competing. The differences among them are within 1 meV/fu when $U \geq 6$. The first two are even almost identical around $U=4$ eV. Clearly, Fig. 4(a) shows that the SC3 is the lowest energy state and its energy is well separated from those of the other three magnetic structures. In the (CuBr)LNO case, similar tiny energy differences but between SC1, SC2, and SC3 are also found. Interestingly, when the FM chain in the CAFM state is set parallel along the a axis, as in SC4, the total energy over the examined U range is much higher than those of the other three configurations, indicating that the Cu ions along the a -axis should not couple ferromagnetically. This finding is contrary to the previous conjecture [21]. The different energy ordering for the four magnetic configurations between the two compounds are conceivable since the magnetic interactions through the path Cu- X -Cu depend subtly on the small structural variation via the X -ion size effect. We will return to this issue in Sec. IIID when considering the various exchange couplings.

B. Atomic structure

Table I lists the fully optimized structural parameters of both materials. For comparison, those obtained by the C4 model are also included. As can be seen in this table, the evaluated lattice constants are in good agreement with the experimental data [24, 25]. The discrepancies between them are only within 1%, the typical errors in the density-functional calculation. The a and b lattice constants of (CuCl)LNO are smaller than those of (CuBr)LNO, which is due primarily to the size effect of Br in the layered structure.

To discuss the structural distortion, we take the (CuCl)LNO case as an example. In the C4 model, copper is in the squeezed octahedral coordination with four long Cu-Cl bonds [$d(\text{Cu-Cl})=2.77 \text{ \AA}$] and two short Cu-O bonds [$d(\text{Cu-O})=1.85 \text{ \AA}$]. The displacements of the Cl and Cu ions in the YY model lead to two shorter Cu-Cl bonds of 2.38 and 2.39 \AA , forming the Cl-Cu-Cl-Cu-Cl zigzag chain to stabilize the structure. The rest two Cu-Cl interatomic distances are increased to 3.27 – 3.29 \AA . In particular, the Cu-O bond length remains short after the structural distortion (from 1.85 \AA to 1.88 \AA), indicating the strong bonding character between Cu and O ions. The calculated interatomic distances are comparable to those reported previously [25]. As a result, the distortion yields the nearly planar CuO_2Cl_2 rather than the octahedral CuO_2Cl_4 environment around the Cu ion (Fig. 5(a)). The resultant CuO_2Cl_2 planar structure is reminiscent of the conventional CuO_4 plaquette, which is commonly observed in copper oxides, e.g., La_2CuO_4 (Ref. [36]) and Sr_2CuO_3 (Ref. [37]). It should be noted that the CuO_2Cl_2 -plaquette zigzag chains was also reported in the TR model [30]. Additionally, the basic electronic structure is similar to that of the CuO_4 planar unit, which will be demonstrated in the next section. Combined with the energetic advantage mentioned above, the YY model provides a realistic description for the atomic structures of (CuCl)LNO and (CuBr)LNO .

From a closer analysis of the positions of all ions in (CuCl)LNO, we found that the distorted atomic structure in the YY model belongs to the space group $Pbam$ (No. 55) [44]. The atomic positions are summarized in Table II. Clearly, the deviations of the Cl ions from the C_4 -symmetry positions are as large as 0.66 \AA , and these values are four times larger than those of Cu ions. Note that the displacements along the a axis are more significant than those along the b axis for both ions to form the zigzag chains.

As expected, the structural distortion on the CuCl plane leads La, Nb and O ions to

shift from the the C_4 -symmetry positions. Figure 5(b) and Table II show the significant tilting and distortion of NbO_6 octahedra. Such a tilting distortion is typical for perovskite oxides structures [45]. Particularly, La ions shift along the b axis by an amount of 0.10 Å. This displacement of La from the C_4 -symmetry positions well agrees with the experimental nonzero value of the EFG tensor at La sites [20], a strong evidence for the structural distortion in (CuCl)LNO. We also found that Nb ions shift along the a axis by a relatively smaller amount of 0.02 Å. Note that the a (b) component of La (Nb) displacement is almost negligible.

Taking into account the tilting of the NbO_6 octahedra in the (CuCl)LNO is important for providing a realistic description of the distortion on the CuCl plane. Figure 5(c), the top view of the atomic structure, clearly demonstrates that the cooperative tilting of the NbO_6 octahedra in the space group $Pbam$ results in a 2×2 periodicity and leads to the zigzag chains with the same periodicity. It is worth pointing out that the higher symmetric 2×1 zigzag chains in the TR model were investigated without consideration of the effect due to the tilting of the NbO_6 octahedra, where these octahedra were still kept at the C_4 tetragonal sites [30]. Allowing the tilting distortion of NbO_6 octahedra in (CuCl)LNO lowers the symmetry of the atomic structure and correspondingly that of the zigzag chains and therefore leads to a lower total energy. In the YY model, the zigzag chains have the glide symmetry about $u = 1/4$ and $v = 1/4$. Specifically, the Cu-Cl bond of 2.39 Å in the zigzag chain is next to the Cl-Cu bond of 2.38 Å in the adjacent chain and vice versa. As compared to those in the TR model, such a *complementary* arrangement between adjacent chains in the YY model allows a further lowering in energy. Now, it is evident that the YY 2×2 model in the present study is energetically more stable than the TR 2×1 one. Similar conclusion holds for (CuBr)LNO.

C. electronic structure

Figure 6 depicts the orbital- and site-projected densities of states (DOS) of (CuCl)LNO with $U=6$ eV, where the valence-band maximum (E_v) is set to zero. The orbitals are projected in the local coordinates with the x and y axes directed to the neighboring Cl ions and the z axis coinciding with the crystal c axis (Fig. 2(b)). Among the major valence state region of 6.3 eV, the higher-energy part consists almost exclusively of O and Cl p

states. There is larger contribution from the Cl p state just below E_v . The lower-energy part, dominated by the Cu d states, is splitted into the doubly occupied dxy , dyz , dzx , $d(x^2 - y^2)$, and singly occupied $d(3z^2 - r^2)$ states. As compared to the GGA DOS (not shown here), the GGA+ U shows an essential redistribution of the Cu $3d$ DOS, i.e., from being above to below the O and Cl p states. That the energy gap (E_g) lies between the occupied anion p states and the unoccupied Cu d states is similar to those in the charge-transfer insulators, e.g., La_2CuO_4 (Ref. [36]) and Sr_2CuO_3 (Ref. [37]). The sharp peak of the low-lying Cu $d(3z^2 - r^2)$ state is a result of the strong bonding between the Cu and O ions with a considerably short Cu-O bond length of 1.88 Å (see Table I). Note that the $d(3z^2 - r^2)$ orbital was hybridized with little Cl p component. The on-site correlation U leads to the half-filling of the $d(3z^2 - r^2)$ orbital, of which the lobes point to the O ions. These results imply a single orbital ground state. Figure 6 shows that, due to the hybridization with the O p state [36], the $d(3z^2 - r^2)$ bonding-antibonding separation (8.3 eV) is larger than the value of U . Therefore, the electronic structure due to the CuO_2Cl_2 plaquette in the YY model is very similar to those of other copper oxides [36] with planar CuO_4 units.

We found that the structural distortion and magnetism together already open up the gap. The E_g of (CuCl)LNO obtained by the GGA is 0.3 eV. However, this result is insufficient to account for the green color appearance [24] of this compound. At $U = 6$ eV, the E_g is increased to 1.8 eV. Further increase of U makes no significant widening for the band gap. The main structures in the DOS of (CuCl)LNO are also found in that of (CuBr)LNO, except for the smaller E_g of 1.5 eV. At this choice of U , the local magnetic moment at the Cu site of (CuBr)LNO is evaluated to be 0.6 Bohr magneton, which agrees with the experiments [21, 29]. An amount of 0.1 Bohr magneton at Br sites is also observed. Hence, we choose the optimal $U = 6$ eV case to discuss the corresponding atomic and electronic properties.

D. exchange interaction

Finally, we discuss the exchange couplings for both (CuCl)LNO and (CuBr)LNO. In the undistorted $C4$ structure, the interactions between the Cu ions can be approximately modeled by the Heisenberg Hamiltonian $\hat{H} = J_1 \sum_{NN} S_i \cdot S_j + J_2 \sum_{2NN} S_i \cdot S_j$, where the sums run over the first and second nearest-neighbor pairs, respectively, and S_i corresponds to the spin moment at site i . The relevant exchange couplings can be then determined by

applying the model to the calculated energies of different spin configurations. For the YY model, the formation of the X -Cu- X -Cu- X zigzag chains along the b axis (Fig. 2(b)) lifts the tetragonal symmetry and leads to inequivalent superexchange pathways, as indicated in Fig. 2. As a result, the J_1 in the C4 structure is split into J_{11} , J_{12} , and J_{13} , with the former two now being the first neighboring inter-chain interactions and the latter the first neighboring intra-chain interaction. The original J_2 coupling is split into two inequivalent J_{21} and J_{22} , which are correspondingly the second neighboring inter-chain interactions. We investigate these interactions via the various spin configurations in Fig. 3. The results are summarized in Table III.

We first discuss the results from the C4 model. Table III shows that J_1 is almost negligible as compared to J_2 . This is reasonable because, as illustrated in Fig. 7(a), there is no overlap between the Cu2 $d(x^2 - y^2)$ and $X4 p$ orbitals. Therefore, even with the obvious overlapping of the Cu1 d and $X4 p$ orbitals, Cu1 and Cu2 could hardly interact with each other. On the other hand, Cu1 can interact with Cu3 via the $X4 p$ orbital.

Based on the $J_1 - J_2$ model, both (CuCl)LNO and (CuBr)LNO were previously claimed [27, 29] to be FM J_1 magnets with competing AFM J_2 interactions, as in the case of $\text{Pb}_2\text{VO}(\text{PO}_4)_2$ (Ref. [18]). Table III indeed shows that $J_1 < 0$ and $J_2 > 0$ for both materials in the C4 model, a direct consequence of the Hund's coupling and virtual electron hopping. However, the recent structural study [21] has raised serious doubt over the validity of the $J_1 - J_2$ model in such materials. Our calculations also indicate that consideration of the structural distortion leads to the opposite results. For (CuCl)LNO, the effective interactions $(J_{11} + J_{12} + 2J_{13})/4$ and $(J_{21} + J_{22})/2$ in the YY model are found to be AFM and FM, respectively. And they both become FM for (CuBr)LNO at large Us . These results come from the complicated interplay between the Hund's coupling, virtual electron hopping, the distorted structure and X -ion size effect. It should be noted that the TR model [30] also results in a leading AFM coupling in (CuCl)LNO. This implies that the simple $J_1 - J_2$ model is unable to describe the present systems. Moreover, the first neighboring interactions become more significant as compared to the second neighboring ones. Figure 7(b) clearly shows that, unlike the C4 case, $\angle \text{Cu1-X4-Cu2}$ is no longer 90° (Table I) due to the structural distortion. This will lead to the overlapping of Cu2 (Cu4) d and $X4 p$ orbitals, and enhance the interaction between Cu1 and Cu2 (Cu4).

In fact, Fig. 8(a) shows that for (CuCl)LNO, $(J_{11} + J_{12})/2 > 0$, $J_{13} > 0$, and

$(J_{21} + J_{22})/2 < 0$ for all the U s considered. It is now clear that, since the interactions due to all the corresponding spin pairs in SC3 satisfy these conditions, (CuCl)LNO in SC3 is much more stable than in the rest three configurations of Fig. 3. Actually, SC3 is the most stable structure among all the spin configurations with the interactions up to second-nearest neighbors. However, by comparing Fig. 8(b) with Fig. 8(a), we found that the J_{13} in (CuBr)LNO becomes FM. This could be ascribed to the fact that the interaction J_{13} depends sensitively on the angle of the Cu1-X4-Cu2 superexchange path in Fig. 7, and the replacement of Cl by Br will change this angle and modify the interaction. Therefore, for (CuBr)LNO, the first neighboring couplings within the chains are FM, and the first two neighboring couplings between adjacent chains are AFM and FM, respectively. None of the four structures in Fig. 3 satisfies these conditions. Specifically, the interactions due to the corresponding spin pairs in SC4 are all opposite to these couplings, giving rise to the result of the SC4 being the highest-energy structure for (CuBr)LNO.

The above analysis seems to indicate that, contrary to previous expectations [20, 26, 27, 29], (CuCl)LNO rather than (CuBr)LNO is less frustrated [29]. To check the reliability of our calculations, we perform the total-energy calculation for an additional structure SC5 with three of the four spins being the same but opposite to the fourth one. For all the possible choices of four magnetic structures containing SC5 in solving the Heisenberg Hamiltonian, the deviations of the relevant couplings (dashed lines in Fig. 8) from those obtained by SC1–SC4 are less than 1.0 meV. More importantly, the signs of these interactions remain unaltered for both materials.

One plausible explanation for the above puzzling discrepancy is that the third neighboring couplings between different zigzag chains [46] may not be completely negligible [27, 30]. Actually, in the YY model, the two CuO_2X_2 plaquettes with the Cu1 and Cu5 ions in Fig. 7(b) could be considered approximately coplanar. Kageyama *et al.* [47] argue that this kind of coplanarity provides an opportunity for the interaction between Cu1 and Cu5 through the overlap of the Cu1 $d(x^2 - y^2)$ -X4 $p - X5 p$ -Cu5 $d(x^2 - y^2)$ orbitals. So, from the structural geometry point of view, such a long-range coupling (8.5 Å) could be possible. However, to examine and identify these couplings, one has to take into account additional eight inequivalent couplings and use a larger supercell whose corresponding calculations are very time-consuming and yet, likely, not accurate enough for the present purposes (Fig. 4). Therefore, we will not address this issue presently. Further theoretical and experimental

work is required to clarify this point.

It is worth pointing out that the first neighboring interactions within the chains and between the adjacent chains have the opposite signs for (CuBr)LNO. The spatial asymmetry of these results again demonstrates the inappropriateness of the square $J_1 - J_2$ model for the Br compound. Furthermore, for both materials, the couplings between the adjacent chains are very competitive to the intra-chain interactions, sharply contrary to the previous conclusion [30]. Tsirlin and Rosner have argued [30] that in the TR model, where the basic structure element is also the CuO_2Cl_2 -plaquette zigzag chain, the large hopping runs along the chain and leads to the strongest interaction. According to their discussion, the inter-chain interaction is rather weak due to the long "nonbonding" Cu-Cl distance and the lack of the proper superexchange path. In the present study, despite the similar backbone in the YY model, the couplings between the adjacent chains are shown to be still substantial. As mentioned before, the strength of exchange interactions between two spin sites should be determined by the overlap of orbitals rather than the distance between them. The interactions between the Cu ions from adjacent chains could be significant through the path mediated by the extended $3p$ orbital of Cl ions (vs O^{2-}) and would be enhanced in the Br case with the further extended $4p$ orbital. Indeed, our calculations show that all the in-plane exchange couplings in (CuBr)LNO are three times larger than those in (CuCl)LNO.

For the inter-layer interaction J_\perp , Table III shows that the J_\perp is AFM, in agreement with the experiment [29]. When compared to the in-plane interaction, the J_\perp in (CuCl)LNO is non-negligible, implying that some long-path (12 Å) interaction between the Cu ions is still cooperative. The origin of this long-range coupling could be associated with the interaction through the Cu $d(3z^2 - r^2)$ orbital. As discussed in Sec. IIIC, this orbital strongly overlaps with the O p_z orbital. The O p_z orbitals further couple with Nb $4d$ orbitals. Therefore, the inter-plane coupling J_\perp shall involve the Cu-O-Nb-O-Nb-O-Cu path. In (CuBr)LNO, however, the coupling is found to be relatively less significant. The strength of all the interactions interested here is decreased with increasing U . The evolution is expected since adding U makes the wavefunctions more localized and the virtual electrons hopping less favorable.

IV. CONCLUSIONS

In conclusion, we have investigated the atomic structure and magnetic property of the copper oxyhalides $(\text{Cu}X)\text{LaNb}_2\text{O}_7$ ($X=\text{Cl}$ and Br) based on the density functional theory. The calculations show that, among the examined structures, the YY 2×2 model proposed by Yoshida *et al.* [20] has the lowest energy. This model is significantly more stable than both the undistorted C4 structure and the TR 2×1 model suggested recently by Tsirlin and Rosner [30]. The X and Cu ions in the YY model are displaced to form the $X\text{-Cu-X-Cu-X}$ zigzag chains and the local environment of copper is distorted to form a nearly CuO_2X_2 plaquette. We found that $(\text{Cu}X)\text{LaNb}_2\text{O}_7$ crystallizes in the space group $Pbam$. The cooperative tilting of the NbO_6 octahedra leads to the lower symmetry of the zigzag chains with a 2×2 periodicity. With consideration of the on-site Coulomb interaction, the YY model shows the single-orbital scenario typical for copper oxides and oxyhalides.

We concluded that $(\text{CuCl})\text{LNO}$ is still the AFM J_1 magnet with mixing FM J_2 interactions. For $(\text{CuCl})\text{LNO}$, the first neighboring interactions within the zigzag chains are AFM, and the first two neighboring couplings between adjacent chains are AFM and FM, respectively. However, the replacement of Cl by Br modifies the first neighboring intra-chain interaction to be FM for $(\text{CuBr})\text{LNO}$. Despite the "well"-separated zigzag chains in the YY model, the couplings between adjacent chains are comparable to those within the chain. The opposite signs of the inter- and intra-chain interactions in $(\text{CuBr})\text{LNO}$ reflect the spatial asymmetry and therefore the failure of the simple $J_1 - J_2$ model for such material. All the in-plane exchange couplings in $(\text{CuBr})\text{LNO}$ are shown to be three times those in the Cl counterpart. It is found that the inter-plane interaction J_\perp is AFM, in agreement with the experiment [29]. The present study strongly suggests that the simple square $J_1 - J_2$ model should be modified to explore the magnetic property of $\text{Cu}X\text{LaNb}_2\text{O}_7$. We hope the present calculations will shed light on the precise crystallographic determination and the magnetic properties of $\text{Cu}X\text{LaNb}_2\text{O}_7$.

Acknowledgments

We are grateful to P. Sindzingre for bringing these systems to our attention. Computer resources provided by the National Center for High-performance Computing are gratefully

acknowledged. This work was supported by the National Science Council and National Center for Theoretical Sciences of Taiwan.

- [1] *Magnetic systems with competing interactions : frustrated spin systems*, edited by H.T. Diep (World Scientific, Singapore, 1994); *Frustrated spin systems*, edited by H.T. Diep (World Scientific, Singapore, 2004).
- [2] E. Dagotto and A. Moreo, Phys. Rev. Lett. **63**, 2148 (1989).
- [3] P. Chandra, P. Coleman, and A. I. Larkin, Phys. Rev. Lett. **64**, 88 (1990).
- [4] R. F. Bishop, D. J. J. Farnell, and J. B. Parkinson, Phys. Rev. B **58**, 6394 (1998).
- [5] R. R. P. Singh, Z. Weihong, C. J. Hamer, and J. Oitmaa, Phys. Rev. B **60**, 7278 (1999).
- [6] L. Capriotti, F. Becca, A. Parola, and S. Sorella, Phys. Rev. Lett. **87**, 097201 (2001).
- [7] O. P. Sushkov, J. Oitmaa, and Z. Weihong, Phys. Rev. B **63**, 104420 (2001).
- [8] J. Sirker, Z. Weihong, O. P. Sushkov, and J. Oitmaa, Phys. Rev. B **73**, 184420 (2006).
- [9] D. Schmalfuß, R. Darradi, J. Richter, J. Schulenburg, and D. Ihle, Phys. Rev. Lett. **97**, 157201 (2006).
- [10] J. R. Viana and J. R. de Sousa, Phys. Rev. B **75**, 052403 (2007).
- [11] A. O'Hare, F. V. Kusmartsev, and K. I. Kugel, Phys. Rev. B **79**, 014439 (2009).
- [12] N. Shannon, B. Schmidt, K. Penc, and P. Thalmeier, Eur. Phys. J. B **38**, 599 (2004).
- [13] N. Shannon, T. Momoi, and P. Sindzingre, Phys. Rev. Lett. **96**, 027213 (2006).
- [14] P. Millet and C. Satto, Mater. Res. Bull. **33**, 1339 (1998).
- [15] R. Melzi, P. Carretta, A. Lascialfari, M. Mambrini, M. Troyer, P. Millet, and F. Mila, Phys. Rev. Lett. **85**, 1318 (2000).
- [16] E. Kaul, Ph.D. thesis, Technische Universität Dresden, Dresden, 2005.
- [17] N. S. Kini, E. E. Kaul, and C. Geibel, J. Phys.: Condens. Matter **18**, 1303 (2006).
- [18] E. E. Kaul, H. Rosner, N. Shannon, R. V. Shpanchenko and C. Geibel, J. Magn. Magn. Mater. **272-276(II)**, 922 (2004).
- [19] Y. Tsujimoto, H. Kageyama, Y. Baba, A. Kitada, T. Yamamoto, Y. Narumi, K. Kindo, M. Nishi, J. P. Carlo, A. A. Aczel, T. J. Williams, T. Goko, G. M. Luke, Y. J. Uemura, Y. Ueda, Y. Ajiro, and K. Yoshimura, Phys. Rev. B **78**, 214410 (2008).
- [20] M. Yoshida, N. Ogata, M. Takigawa, J. Yamaura, M. Ichihara, T. Kitano, H. Kageyama, Y.

- Ajiro, K. Yoshimura, *J. Phys. Soc. Jpn.* **76**, 104703 (2007).
- [21] M. Yoshida, N. Ogata, M. Takigawa, T. Kitano, H. Kageyama, Y. Ajiro, K. Yoshimura, *J. Phys. Soc. Jpn.* **77**, 104705 (2008).
- [22] A. I. Liechtenstein, V. I. Anisimov, and J. Zaanen, *Phys. Rev. B* **52**, R5467 (1995).
- [23] T. A. Kodenkandath, J. N. Lalena, W. L. Zhou, E. E. Carpenter, C. Sangregorio, A. U. Falster, W. B. Simmons, C. J. O'Connor, J. B. Wiley, *J. Am. Chem. Soc.* **121**, 10743 (1999).
- [24] T. A. Kodenkandath, A. S. Kumbhar, W. L. Zhou, and J. B. Wiley, *Inorg. Chem.* **40**, 710 (2001).
- [25] G. Caruntu, T. A. Kodenkandath, J. B. Wiley, *Mater. Res. Bull.* **37**, 593 (2002).
- [26] H. Kageyama, J. Yasuda, T. Kitano, K. Totsuka, Y. Narumi, M. Hagiwara, K. Kindo, Y. Baba, N. Oba, Y. Ajiro, and K. Yoshimura, *J. Phys. Soc. Jpn.* **74**, 3155 (2005).
- [27] H. Kageyama, T. Kitano, N. Oba, M. Nishi, S. Nagai, K. Hirota, L. Viciu, J. B. Wiley, J. Yasuda, Y. Baba, Y. Ajiro, and K. Yoshimura, *J. Phys. Soc. Jpn.* **74**, 1702 (2005).
- [28] M. H. Whangbo and D. Dai, *Inorg. Chem.* **45**, 6227 (2006).
- [29] N. Oba, H. Kageyama, T. Kitano, J. Yasuda, Y. Baba, M. Nishi, K. Hirota, Y. Narumi, M. Hagiwara, K. Kindo, T. Saito, Y. Ajiro, and K. Yoshimura, *J. Phys. Soc. Jpn.* **75**, 113601 (2006).
- [30] A. A. Tsirlin and H. Rosner, *Phys. Rev. B* **79**, 214416 (2009).
- [31] S. C. Erwin, *Phys. Rev. Lett.* **91**, 206101 (2003).
- [32] A. Malashevich and D. Vanderbilt, *Phys. Rev. Lett.* **101**, 037210 (2008).
- [33] H. Rosner, R. R. P. Singh, W. H. Zheng, J. Oitmaa, S. -L. Drechsler, and W. E. Pickett, *Phys. Rev. Lett.* **88**, 186405 (2002).
- [34] J. P. Perdew, K. Burke, and M. Ernzerhof, *Phys. Rev. Lett.* **77**, 3865 (1996).
- [35] F. C. Zhang and T. M. Rice, *Phys. Rev. B* **37**, 3759 (1988).
- [36] M. T. Czyżyk and G. A. Sawatzky, *Phys. Rev. B* **49**, 14211 (1994).
- [37] W. C. Mackrodt and H. J. Gotsis, *Phys. Rev. B* **62**, 10728 (2000).
- [38] I. Solovyev, N. Hamada, and K. Terakura, *Phys. Rev. B* **53**, 7158 (1996).
- [39] G. Kresse and D. Joubert, *Phys. Rev. B* **59**, 1758 (1999).
- [40] G. Kresse and J. Furthmüller, *Comput. Mater. Sci.* **6**, 15 (1996).
- [41] A. Kitada, Y. Tsujimoto, H. Kageyama, Y. Ajiro, M. Nishi, Y. Narumi, K. Kindo, M. Ichihara, Y. Ueda, Y. J. Uemura, and K. Yoshimura, *Phys. Rev. B* **80**, 174409 (2009).

- [42] The model in Ref. [43] originally proposed for $(\text{FeCl})\text{LaNb}_2\text{O}_7$ (the same shown in Fig. 16(a) of Ref. [20]) is energetically less favorable than the YY model.
- [43] N. Oba, H. Kageyama, T. Saito, M. Azuma, W. Paulus, T. Kitano, Y. Ajiro, and K. Yoshimur, *J. Magn. Magn. Mater.* **310**, 1337 (2007).
- [44] *International Tables for Crystallography*, edited by T. Hahn (Kluwer, Dordrecht, 1989), Vol. A.
- [45] *Colossal Magnetoresistance, Charge Ordering, and Related properties of Manganese Oxides*, edited by C. N. R. Rao and B. Raveau (World Scientific, Singapore, 1998).
- [46] From the viewpoint of the square $J_1 - J_2$ model, these interactions should be regarded as the fourth-nearest-neighbor interactions.
- [47] H. Kageyama, J. Kang, C. Lee, and M.-H. Whangbo, (unpublished).

FIGURE CAPTIONS

Fig. 1: (Color online) Crystal structure of $(\text{Cu}X)\text{LaNb}_2\text{O}_7$ ($X=\text{Cl}, \text{Br}$) in the tetragonal space group P_4/mmm .

Fig. 2: (Color online) (a) The undistorted tetragonal model and (b) the distorted model proposed by Yoshida *et al.* [20] for $(\text{Cu}X)\text{LaNb}_2\text{O}_7$ ($X=\text{Cl}, \text{Br}$). Large and small spheres denote X and Cu ions, respectively. The relevant exchange couplings are also indicated.

Fig. 3: (Color online) The four different spin configurations of Cu ions considered in the present study. Large and small spheres denote Cl/Br and Cu ions, respectively.

Fig. 4: (Color online) Total energies of (a) $(\text{CuCl})\text{LaNb}_2\text{O}_7$ and (b) $(\text{CuBr})\text{LaNb}_2\text{O}_7$ in the spin configurations shown in Fig. 3. The energies are relative to that of SC2.

Fig. 5: (Color online) Perspective view of (a) the CuO_2X_2 -plaquette zigzag chains and (b) tilted NbO_6 octahedra of $(\text{Cu}X)\text{LaNb}_2\text{O}_7$ ($X=\text{Cl}, \text{Br}$) in the space group $Pbam$. (c) Top view of (b). Here, the symbols for the various atomic species are the same as those in Fig. 1.

Fig. 6: (Color online) Orbital- and site-projected density of states (DOS) of $(\text{CuCl})\text{LaNb}_2\text{O}_7$, obtained by $U = 6$ eV and SC2 in Fig. 3. The energy is relative to the valence-band maximum.

Fig. 7: (Color online) Schematic plot of Cu $d(x^2 - y^2)$ and X p orbitals of $(\text{Cu}X)\text{LaNb}_2\text{O}_7$ ($X=\text{Cl}, \text{Br}$) in the space group (a) P_4/mmm and (b) $Pbam$.

Fig. 8: (Color online) The U -dependence of the in-plane exchange couplings of (a) $(\text{CuCl})\text{LaNb}_2\text{O}_7$ and (b) $(\text{CuBr})\text{LaNb}_2\text{O}_7$. The solid lines are calculated from SC1–SC4 in Fig. 3. The dashed lines show the uncertainty of the calculations. See the text for details. Note that the scale of exchange coupling in (a) is only half of that in (b).

FIG. 1:

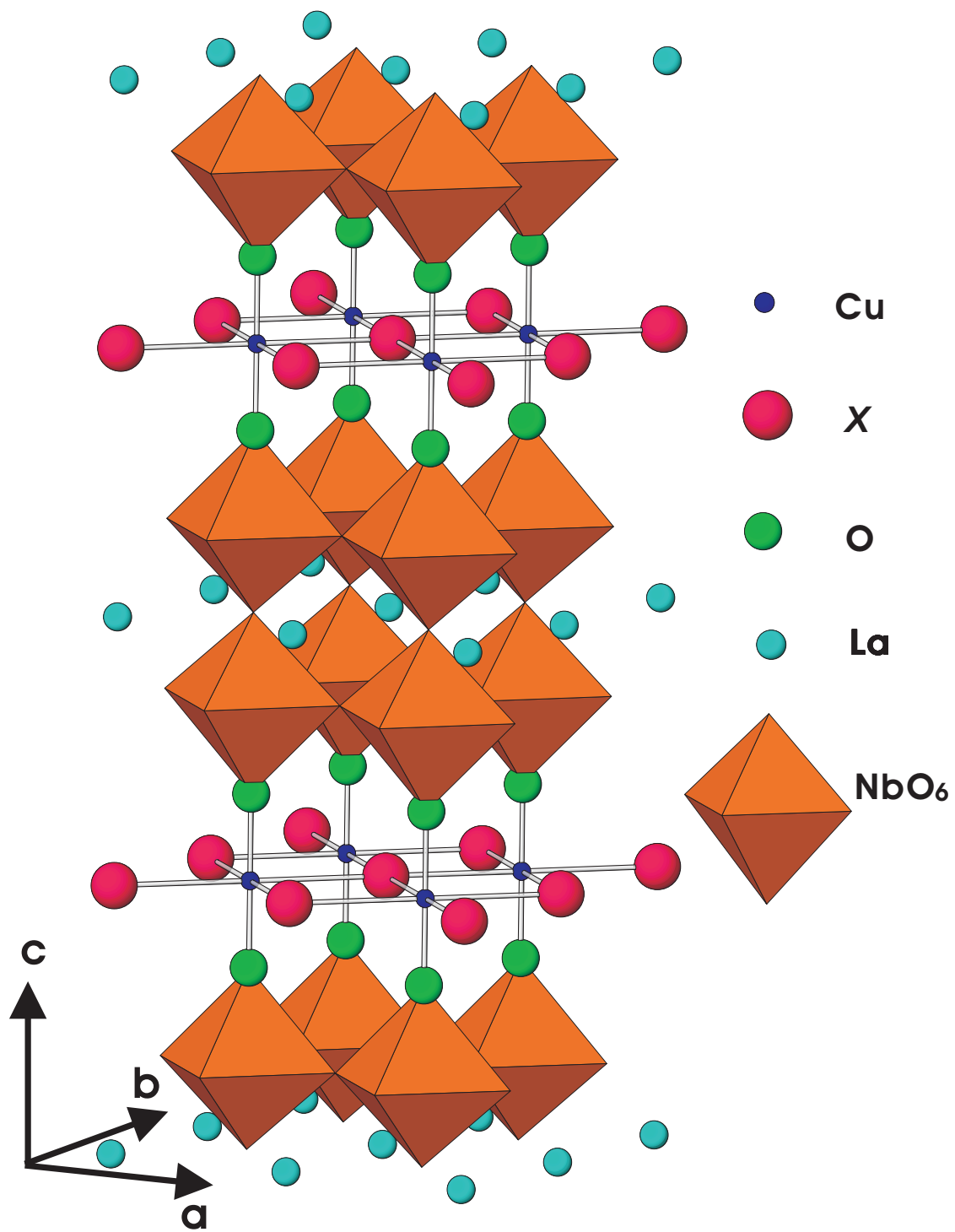


FIG. 2:

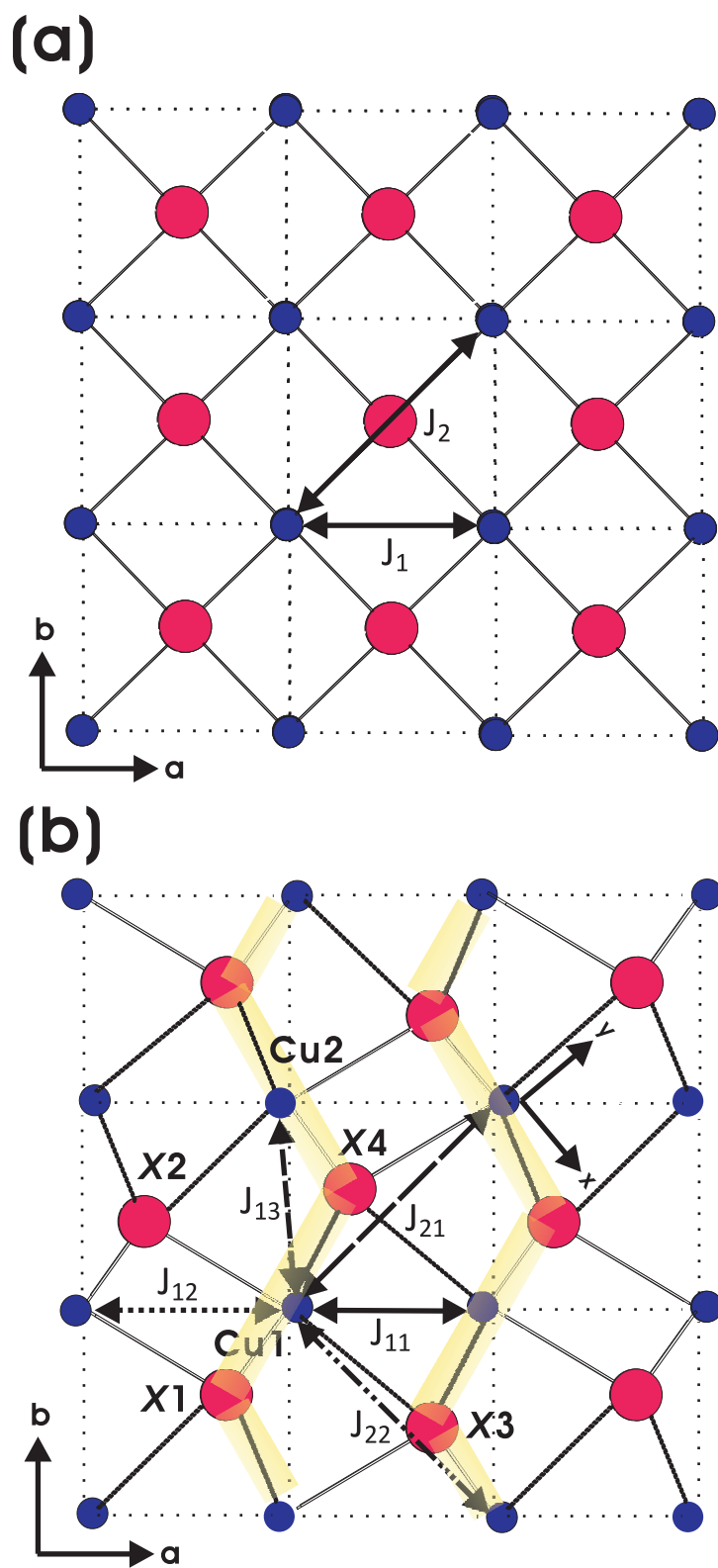


FIG. 3:

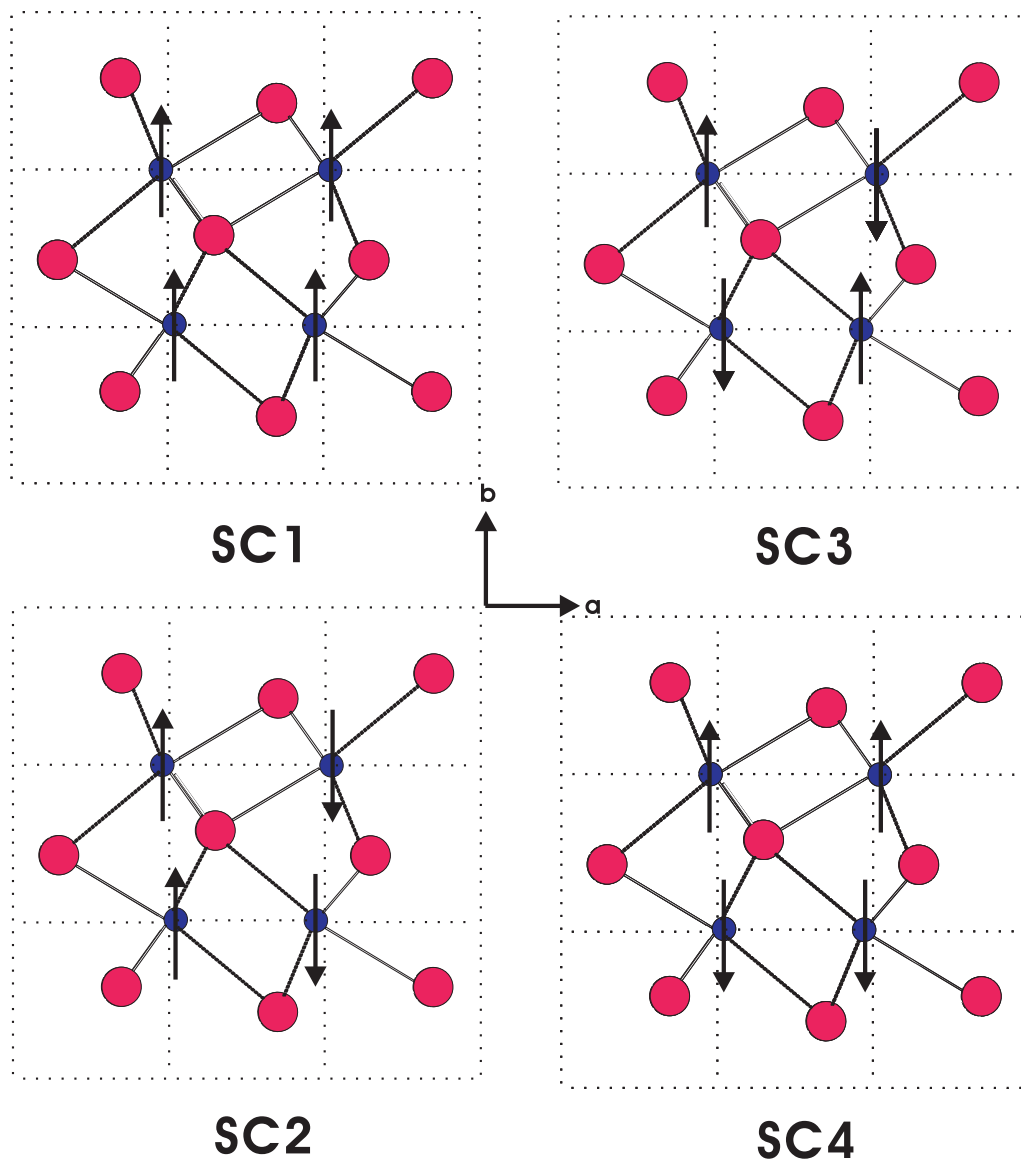


FIG. 4:

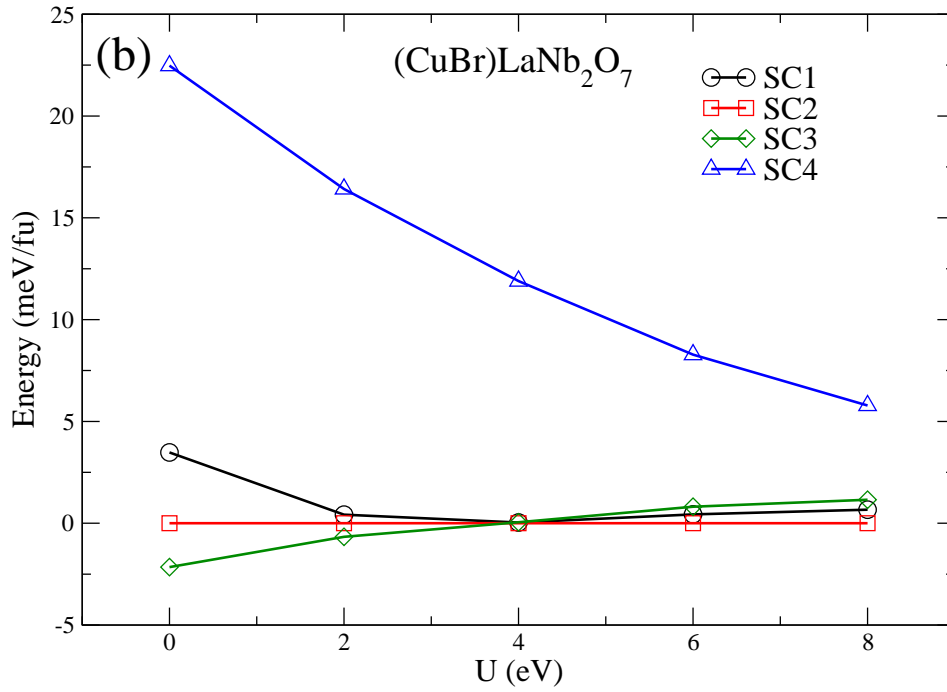
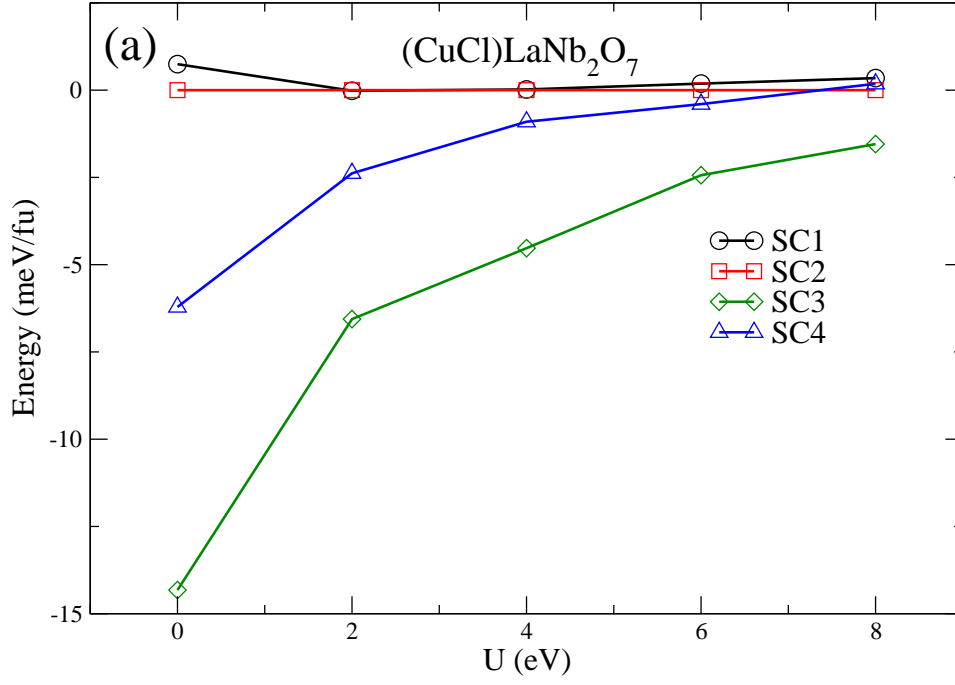


FIG. 5:

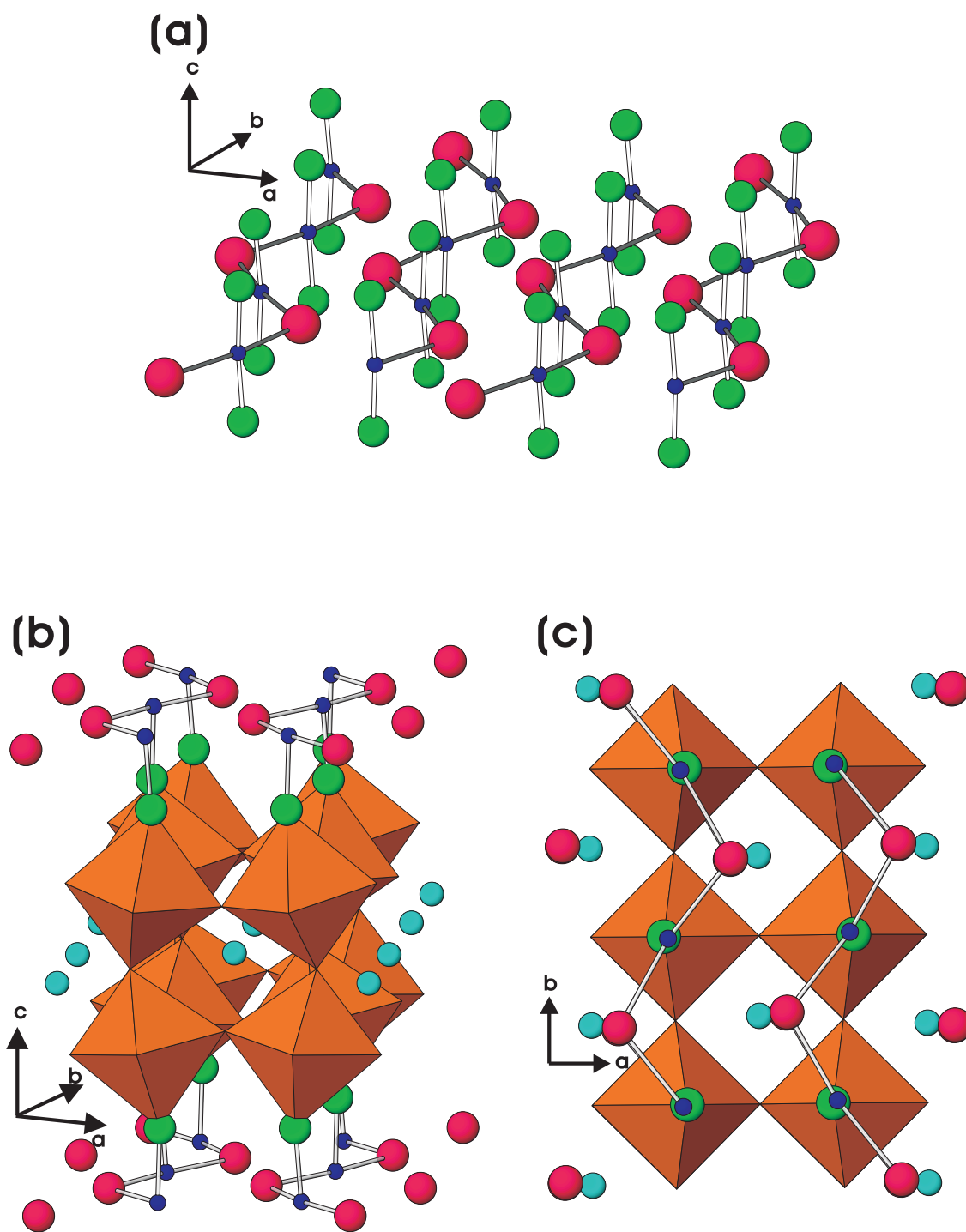


FIG. 6:

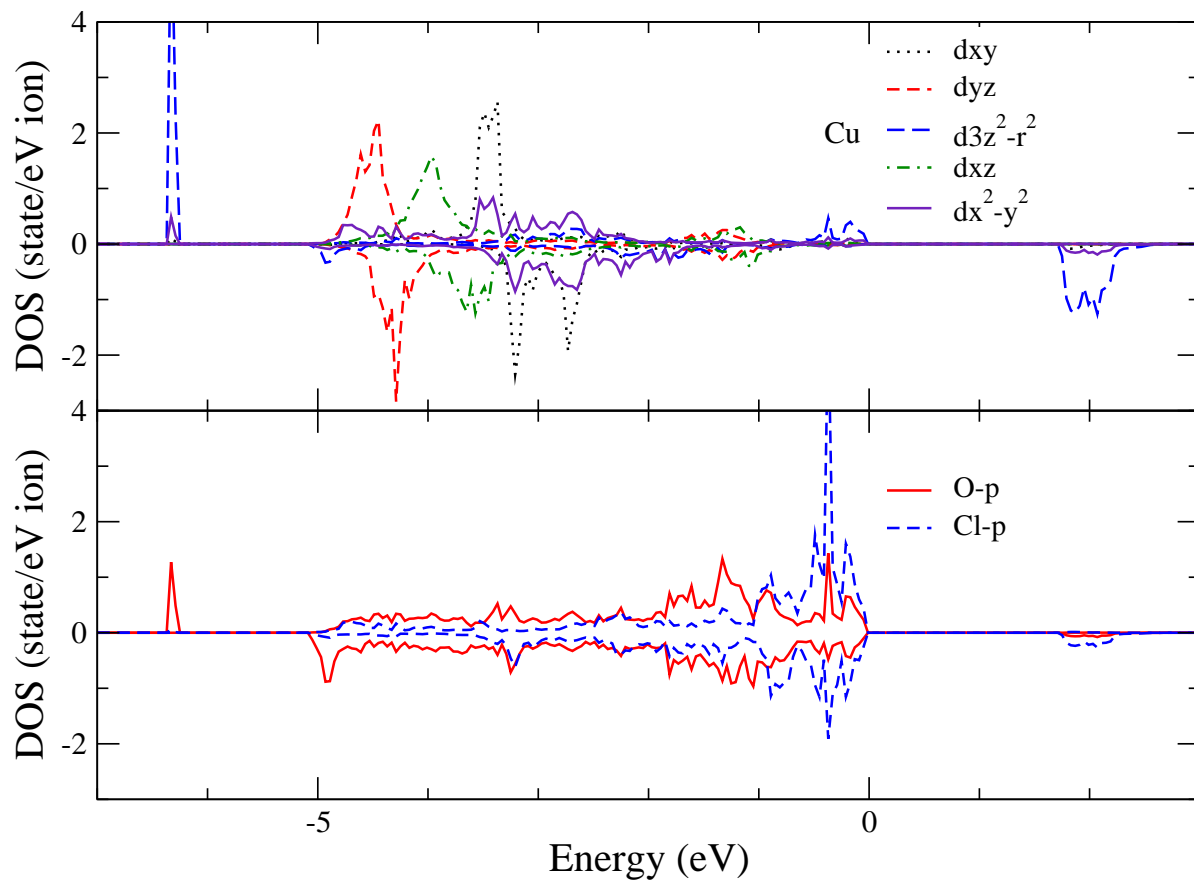


FIG. 7:

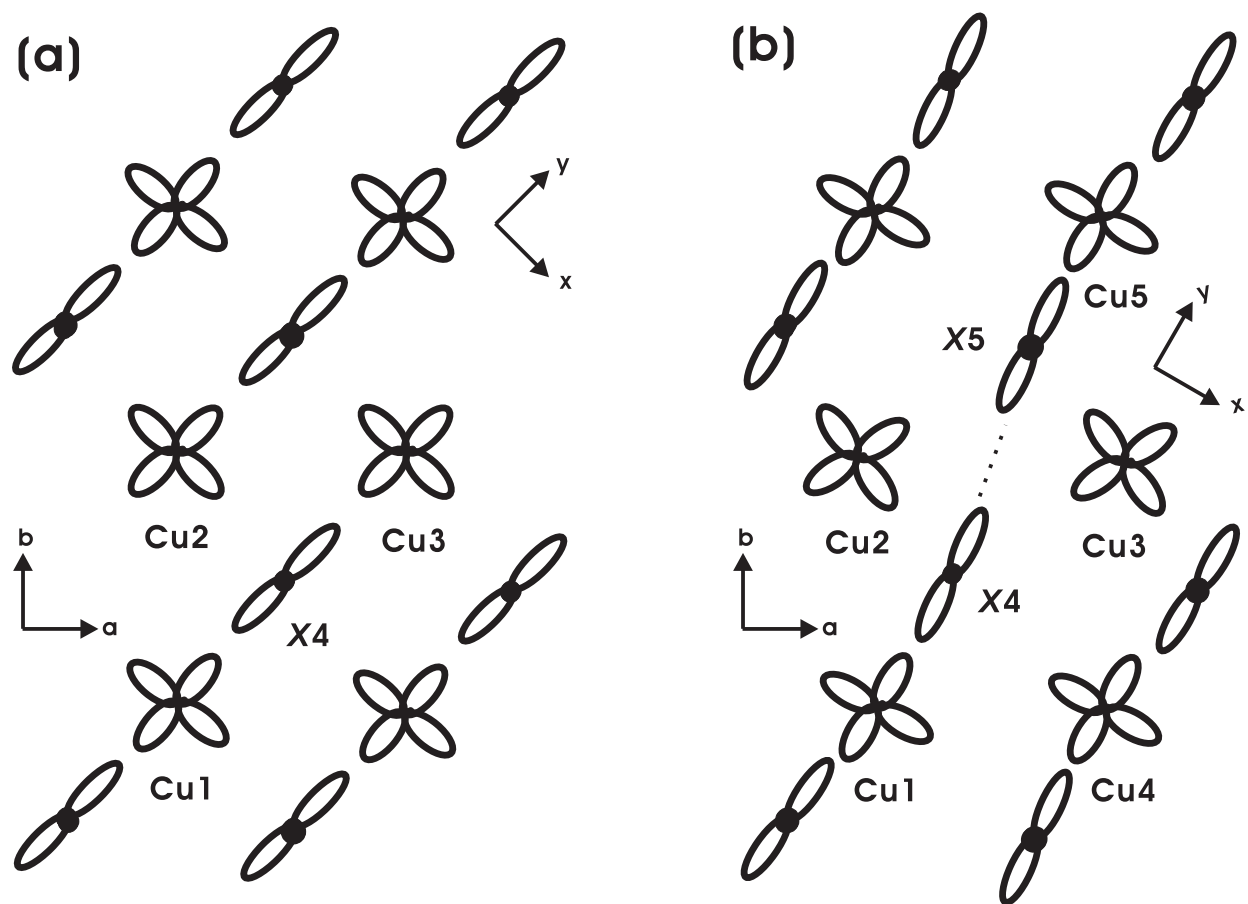


FIG. 8:

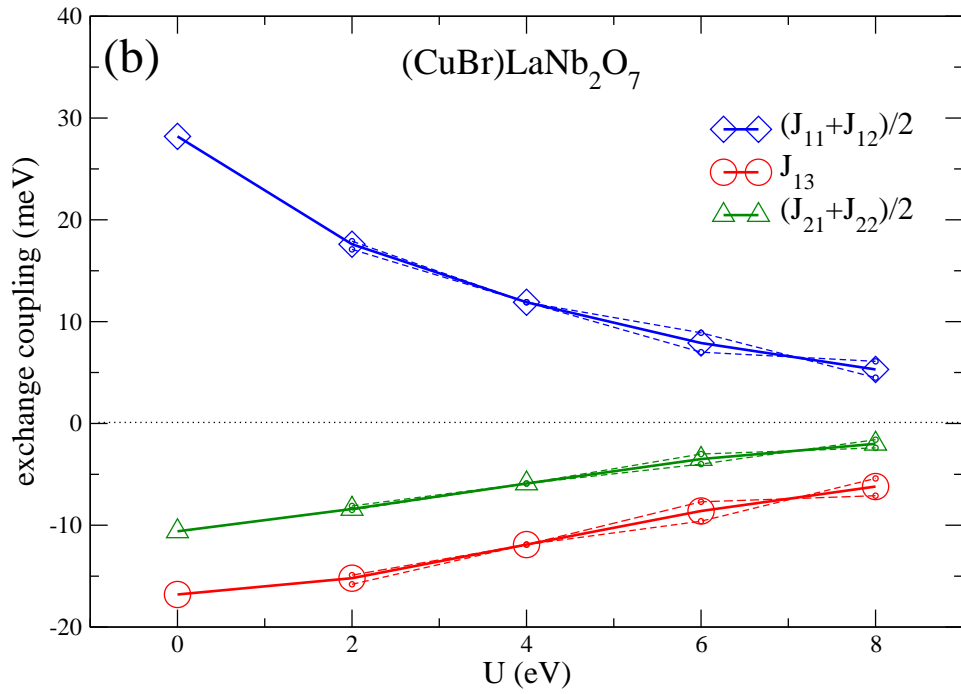
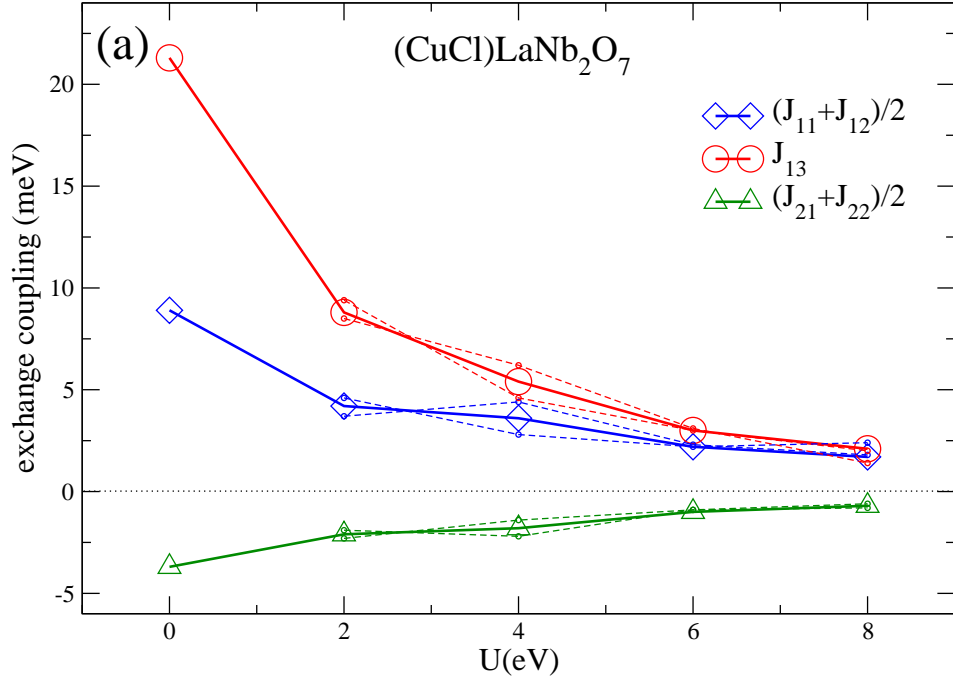


TABLE I: The calculated lattice constants (\AA), relevant interatomic distances (\AA), and bond angles ($^\circ$) of $(\text{Cu}X)\text{LaNb}_2\text{O}_7$ ($X=\text{Cl}, \text{Br}$), obtained by $U = 6$ eV and SC2 in Fig. 3. The latter two refer to those in Fig. 2(b). In the bottom part, the results in the undistorted tetragonal model are listed for comparison. The values in parentheses are the corresponding experimental data.

	(CuCl)LaNb ₂ O ₇	(CuBr)LaNb ₂ O ₇
a	7.868	7.889
b	7.883	7.914
c	11.878	11.853
Cu1- X 1	2.39 (2.40 [†])	2.54
Cu1- X 2	3.27 (3.14 [†])	3.11
Cu1- X 3	3.29	3.11
Cu1- X 4	2.38	2.52
Cu1-O	1.88 (1.84 [†])	1.88
\angle X 1-Cu1- X 2	83.6	81.5
\angle X 2-Cu1- X 4	87.1	88.8
\angle X 4-Cu1- X 3	102.7	101.3
\angle X 3-Cu1- X 1	86.6	88.3
\angle Cu1- X 4-Cu2	112.2	103.4
a^*	3.914 (3.884 [†])	3.942 (3.899 ^{††})
c^*	11.892 (11.736 [†])	11.853 (11.706 ^{††})
Cu- X^*	2.77	2.79
Cu-O*	1.85	1.87

†: Ref. [25]

††: Ref. [24]

TABLE II: The calculated atomic structural parameters of $(\text{Cu}X)\text{LaNb}_2\text{O}_7$ ($X=\text{Cl}$ and Br) in the space group $Pbam$, obtained by $U = 6$ eV and SC2 in Fig. 3. u , v , and w denote fractional coordinates based on the a , b , and c lattice constants, respectively.

ion	site	$(\text{CuCl})\text{LaNb}_2\text{O}_7$			$(\text{CuBr})\text{LaNb}_2\text{O}_7$		
		u	v	w	u	v	w
Cu	$4h$	0.2706	0.0077	0.5	0.2720	0.0057	0.5
X	$4h$	0.4185	0.2711	0.5	0.4481	0.2713	0.5
La	$4g$	0.5000	0.2622	0	0.5000	0.2624	0
Nb	$8i$	0.2522	0.0000	0.1911	0.2520	0.9998	0.1903
O1	$4f$	0.5	0	0.1336	0.5	0	0.1334
O2	$4e$	0	0	0.1841	0	0	0.1834
O3	$8i$	0.2498	0.2501	0.1522	0.2498	0.2499	0.1520
O4	$4g$	0.2004	0.0001	0	0.2004	0.0000	0
O5	$8i$	0.2830	0.0008	0.3417	0.2818	0.0000	0.3413

TABLE III: The exchange couplings (meV) of (CuCl)LaNb₂O₇ and (CuBr)LaNb₂O₇. The notation is explained in the text. U (eV) is the on-site Coulomb correlation interaction.

U	(CuCl)LaNb ₂ O ₇						(CuBr)LaNb ₂ O ₇					
	$(J_{11} + J_{12})/2$	J_{13}	$(J_{21} + J_{22})/2$	J_{\perp}	J_1	J_2	$(J_{11} + J_{12})/2$	J_{13}	$(J_{21} + J_{22})/2$	J_{\perp}	J_1	J_2
0	8.9	21.3	-3.7	5.1	-1.8	18.4	28.2	-16.8	-10.6	5.4	-2.9	-1.5
4	3.6	5.4	-1.8	2.0	-3.6	26.9	11.9	-11.9	-5.9	2.2	-1.8	23.3
6	2.2	3.0	-1.0	1.3	-2.5	19.4	7.9	-8.6	-3.5	1.5	-0.1	25.5
8	1.7	2.1	-0.7	0.7	-1.7	13.5	5.3	-6.2	-2.0	0.9	-0.3	18.6